Taylor & Francis
Taylor & Francis Group

# A Wide-Range Controlling of Optical and Morphological Parameters of PDLC Samples via the Intensity of Curing Light

## F. Z. ELOUALI,[1] O. YAROSHCHUK,[1,2] AND U. MASCHKE[1]

[1]Equipe Ingénierie des Systèmes Polymères, UMET, UMR N° 8207 CNRS, Université des Sciences et Technologies de Lille, Villeneuve d'Ascq Cedex, France
[2]Institute of Physics, NASU, Prospect Nauki, Kyiv, Ukraine

*The phase separation kinetics and morphology of polymer dispersed liquid crystals (PDLCs) formed from the nematic liquid crystal (LC) E7 and pre-polymeric composition NOA65 via the photoinduced phase separation in a wide intensity range of actinic UV light ($I = 0.5–40\,mW/cm^2$) are investigated. The phase separation process was monitored by measuring transmittance kinetics of the composite layers, while the morphology was observed by polarized optical microscopy. Increase of curing light intensity dramatically influenced the phase separation kinetics and final structure of PDLC samples. Reduction of light intensity below $2\,mWcm^{-2}$ resulted in transition from the conventional PDLC morphology of fine monodispersed LC droplets (with a droplet diameter $d \sim 1\,\mu m$) to the morphology of large LC domains ($d \sim 10\,\mu m$) of irregular shape. The realized transition extends the field of PDLC morphologies of E7-NOA65 composites and thus the field of their potential applications.*

**Keywords** E7; liquid crystals; morphology; NOA65; PDLC

**PACS** 42.70.Df; 42.79.Kr; 61.30.Pq

## 1. Introduction

The liquid crystal (LC) – polymer composites are the most extensively studied LC composites operating in a light scattering mode. In the most common case they consist of isolated or connected LC droplets dispersed in a rigid polymer matrix.

Because of this morphology they are usually named "polymer dispersed liquid crystals" (PDLCs). In a zero-field state PDLC layers intensively scatter light due to refractive index mismatch between the LC droplets and polymer matrix, adjacent droplets and within the droplets of LC [1]. In the electric or magnetic field the PDLC layers become transparent due to the field induced alignment of LC within the droplets leading to matching the refractive indices of LC and polymer. The transparent state of PDLC films can also be achieved by heating them above the clearing

---

temperature of LC. This effect is also caused by a convergence of refractive indices of LC and polymer and vanishing of scattering components caused by anisotropy of LC. Based on electrically and thermally controlled light scattering effects in PDLCs, a large number of devices is developed such as smart windows, displays, optical valves, tunable LC lenses, etc. [1–3].

Most commonly, PDLC are formed through a polymerization-induced phase separation (PIPS). In this method a homogeneous mixture of LC and pre-polymer composition (monomers, oligomers, initiators, etc.) is subjected to polymerization/ crosslinking reactions using light or e-beam irradiation, heating and polycondensation. The polymer phase hardening in a course of phase separation ejects LC promoting its microencapsulation.

The polymerization of pre-polymeric compositions commonly used in PIPS PDLCs is based on free radical polymerization. Among these compositions two classes are most frequently used. The first class comprises thiol-ene mixtures undergoing step-growth polymerization under irradiation, while the other class includes acrylate compositions capable to polymerize via chain-growth radical polymerization [4]. Comparing with acrylate systems, the thiol-ene compositions provide much lower shrinkage non-uniformity and precise control of PDLC morphology. In holographic type PDLCs they provide high diffraction efficiency and switching contrast [5]. This explains especial interest to thiol-ene compositions as polymer binders for PDLCs.

The commonly used thiol-ene based PDLCs are made of commercial optical adhesive NOA65 from Norland Products and the cyano-n-phenyl LC mixtures, usually E7, from Merck. The NOA65 pre-polymer is a UV curable pre-polymer mixture containing trifunctional thiol and a tetrafunctional urethane allyl ether (the ene) [6]. The ordinary refractive index of LC E7 and refractive index of NOA65 are favorably very close [7] so that corresponding PDLC films become fully transparent in a field on state. The early studies of such PDLCs were focused on maximal improvement of their electro-optic performance based on optimization of curing conditions (UV exposure, curing temperature, polymer concentration, etc.) [8–11]. The curing reactions and phase separation kinetics in NOA65-E7 composites were in-depth studied by Koenig's group using real-time FTIR spectroscopy [12–14]. Recently, T. White *et al.* [15] considered effect of functionality of thiol and ene monomers on polymerization kinetics and morphology of PDLC composites. It was found that increasing monomer functionality (both thiol and ene) reduces gel point conversion of thiol-ene polymer and thus the size of phase separated LC domains in PDLC samples. This gives additional possibility for optimization of thiol-ene based PDLCs.

However, as recently shown, essential gap for further improvement of NOA65-E7 composites still exists without chemical modification of polymer composition. This might be achieved by thorough optimization of NOA65 and E7 composition, processing parameters and, possibly, insertion of some additional components. In [16,17] we demonstrated that doping NOA65-E7 PDLCs with nanoparticles of inorganic materials may substantially increase electro-optic contrast and reduce the off-axis haze. The morphological evolution of this system with a wide-range change of polymer concentration $C_p$ was elucidated in [18].

The present study considers the phase separation kinetics and the morphology of NOA65-E7 PDLCs as functions of curing light intensity. By using an intensity range much wider than in the early studies of these composites [9,11], several types of PDLC morphologies were found. In situ monitoring of phase separation allowed us to determine parameters of this process as functions of curing light intensity.

## 2. Experimental

### 2.1. *Samples*

As LC component of PDLCs we used nematic LC E7 (BDH/Merck), an eutectic mixture of cyanobiphenyls with the nematic mesophase in the range $(-30)$–$(+61)°C$ [12,13]. The polymer binder was a UV curable optical adhesive NOA65 (Norland Products), a mixture of trimethylolpropane diallyl ether, trimethylolpropane tris thiol, isophorone diisocyanate ester, and benzophenone as photoinitiator [6,12].

60 wt.% of E7 and 40 wt.% of NOA65 were automatically thoroughly mixed over 10 h at room temperature and used as the initial reactive mixture for UV curing. Samples were prepared by sandwiching the initial reactive mixture between two glass plates containing transparent ITO electrodes. The gap between the substrates was $d = 26 \pm 2\,\mu m$. The UV light source was a lamp LC3 from Hamamatsu. The curing light intensity, $I$, detected in the spectral range 250–400 nm, was $0.5-40\,mWcm^{-2}$. The basic curing time was fixed at 70 s.

### 2.2. *Experimental Techniques*

The optical studies were carried out by using experimental set up earlier described in [19]. The system measures transmission of PDLC samples for unpolarized He-Ne laser light at $\lambda = 632.8$ nm impinging normally on the samples. The distance between the sample and the detector was set approximately at 30 cm to have collection angle of the transmitted light about $\pm 2°$.

The phase separation kinetics was studied by monitoring optical transmittance of PDLC samples, $T$, in a course of UV irradiation. The angle of incidence of UV light on the sample was about $30°$. The light intensity was changed by changing distance between the UV source and the sample. The exposure process was launched 20 s after starting recording of sample transmittance. After 70 s of exposure the sample was monitored additionally 2500 s to clarify a post-irradiation behavior.

The microscopic observations were carried out by using a polarizing optical microscope Olympus BX41 equipped with a digital camera conjugated with a PC.

## 3. Results and Discussion

### 3.1. *Transmittance Kinetics*

Figure 1 shows transmittance kinetics for two distinctly different intensities of curing light. The arrows with marks ON and OFF point the instants of time when the UV light is switched on and off. The parts of $T(t)$ curves corresponding to illumination phase are collected in Figure 2.

One can notice that sample transmittance monotonically decays with the exposure time demonstrating trend of saturation. The higher is intensity of UV light the faster is decay of $T$. This behavior is typical for PDLCs formed by PIPS [2,3].

In general, the measured transmittance vs. exposure time curves cannot be satisfactorily fitted by a single exponential function. Firstly, the $T(t)$ curves for low intensities contain specific initial tail with a constant transmittance followed by a low rate of transmittance decay. Secondly, $T(t)$ curves for high intensities usually undergo maximum in the final part of intensity decay (see inset to Fig. 1a), which might be caused by nematic to isotropic phase transition in LC droplets.
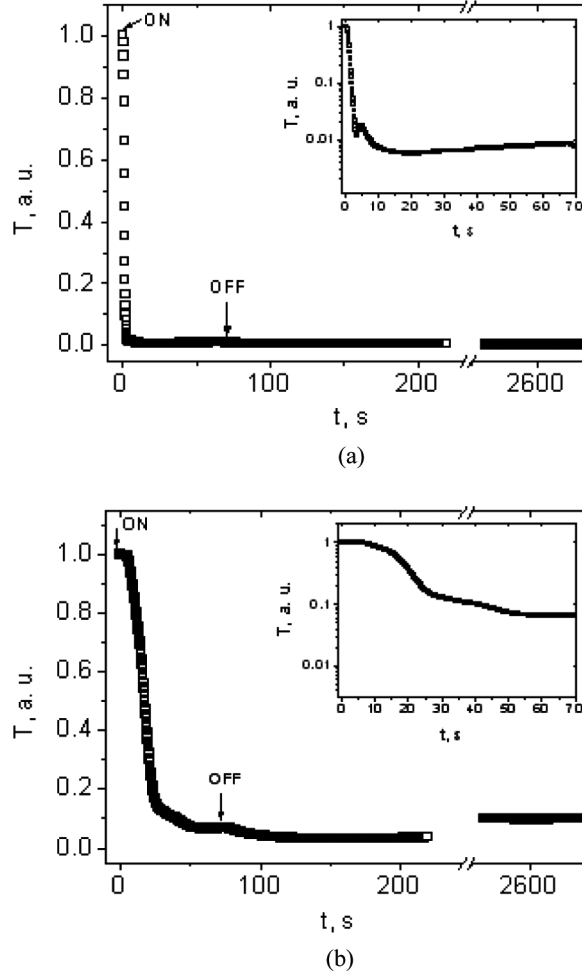
**Figure 1.** Transmittance kinetic curves for UV light intensity $36\,\text{mWcm}^{-2}$ (a) and $0.8\,\text{mWcm}^{-2}$ (b). The arrows with marks ON and OFF point the instants of time when the illumination and relaxation phases of $T(t)$ curves are started. The insets present parts of $T(t)$ curves corresponding to the illumination phase on a logarithmic scale.

Because this maximum is small, it will be further ignored in the fitting process. Using this simplification, $T(t)$ curves can be satisfactorily fitted by a stretched exponent commonly used to describe complex relaxation processes, for instance, relaxation in disordered systems [20]:

$$T = T_0 + A \exp(-(t/\tau_s)^{\beta}) \tag{1}$$

In Eq. (1) $T_0$ is a transmittance value in saturation state, $\tau_s$ is a decay time, $A$ is a value of transmittance decay and $\beta$ is a stretching parameter. Figure 2 demonstrates that Eq. (1) fits experimental curves very well except the last parts of these curves corresponding to final 10–15% of decay. The fitting parameters corresponding to different intensities of curing light are summarized in Table 1. This table also
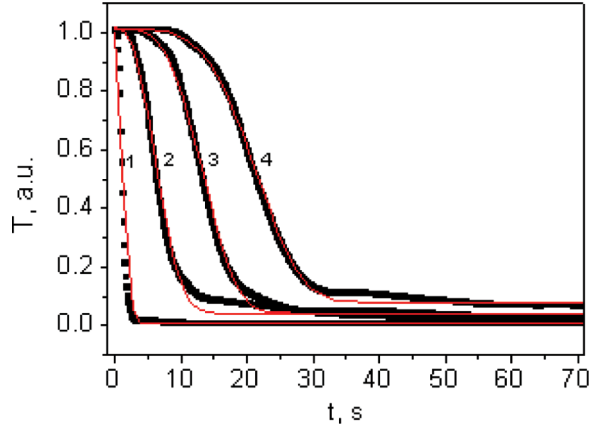
**Figure 2.** Measured (filled squares) and fitted (continuous lines) $T(t)$ curves corresponding to the illumination phase. The fitting is provided by Eq. (1). The curves (1), (2), (3) and (4) correspond to UV light intensities of 36, 4, 2 and $0.8\,\mathrm{mWcm}^{-2}$, respectively.

includes a mean decay time calculated as:

$$\langle\tau\rangle = \int_0^\infty dt \exp(-(t/\tau_s)^\beta), \qquad (2)$$

where $\tau_s$ and $\beta$ are parameters preliminarily determined by fitting. As can be seen from Table 1, the values of $<\tau>$ are close to $\tau_s$.

Moreover, growing of curing light intensity $I$ results in monotonous decrease and saturation of $\beta$, $<\tau>$ and $T_0$. The possible reasons of these trends are considered below.

At high intensities, $\beta$ approaches 1 so that a photoinduced decay of $T$ is roughly a single exponential function. In this case the decay of $T$ starts practically instantly with illumination. To the contrary, lowering of $I$ enhances stretching of $T(t)$ curve; for intensities higher than $2\,\mathrm{mW/cm}^2$ stretching parameter $\beta$ exceeds 4. The pronounced tail observed in the initial phase of these curves means that response of $T$ on illumination is essentially delayed.

**Table 1.** Fitting parameters for $T(t)$ curves corresponding to different intensities of curing light

| UV light intensity | Fitting parameters | | | | |
|---|---|---|---|---|---|
| | $A$ | $\tau$ | $\beta$ | $T_0$ | $<\tau>$ |
| 0.48 | 0.92 | 24.2 | 4.4 | 0.088 | 20.4 |
| 0.8 | 0.93 | 23.1 | 4.3 | 0.081 | 19.7 |
| 1.2 | 0.94 | 1 | 4.0 | 0.062 | 18.6 |
| 2 | 0.96 | 14.7 | 3.7 | 0.042 | 13.2 |
| 4 | 0.97 | 7.5 | 2.6 | 0.035 | 6.9 |
| 18 | 0.99 | 2.8 | 2.2 | 0.014 | 2.6 |
| 36 | 1 | 1.5 | 1.8 | 0.008 | 1.27 |

The marked difference in the initial parts of $T(t)$ curves can be explained assuming difference in the phase separation mechanisms for high and low intensities of curing light. At high intensities, the gel point of prepolymer is quickly reached so that the phase separation occurs mainly via a liquid-gel separation process. At low intensity, much longer time is needed for reaching gel point of prepolymer at which intensive separation is started. This might explain specific tail of $T(t)$ curves detected for the samples prepared at low intensity. Since viscosity of prepolymer binder changes slowly, one can assume that the initial transmittance decay, i.e., initial tail of $T(t)$ curves, is caused by a liquid-liquid separation mechanism. At longer exposure, the gel point is reached resulting in intensive liquid-gel separation. Decrease of $<\tau>$ with the intensity of curing light reflects a shortening of both gelation time and liquid-gel separation time. The difference in the initial separation process may explain essential difference in the morphology of PDLC samples discussed in the next section.

Decrease of $T_0$ with the intensity $I$ implies enhancement of light scattering in a zero field. It is worthwhile noting that the increase of exposure time from 70 to 500 s did not essentially change the value of $T_0$. This means that 70 s is the time sufficient for phase separation in our composites.

Finally the part of transmittance kinetics after the UV irradiation is shut down (the relaxation part, Fig. 1) should be analyzed. There is obvious that at $I > 2\,\mathrm{mWcm}^{-2}$ sample transmittance $T$ does not practically change after the irradiation was turned off. In case of lower light intensity, the transmittance $T$ demonstrates insufficient change (10–15% of its maximal value). Usually, $T$ slightly decreases and then grows up and saturates as demonstrated in Figure 1b. These changes are rather slow compared with the transmittance decay under illumination. The relaxation behavior in case of 500 s exposure time was rather similar to that in case of 70 s exposure time. The observation of PDLC samples using polarizing optical microscope immediately after UV illumination showed that the slow dynamics of $T$ can be caused by a coalescence of LC drops and establishment of equilibrium director configuration within these drops.

## 3.2. PDLC Morphologies

Figure 3 illustrates microscopic pictures of PDLC samples formed by different intensities of curing light. Similar as in case of $T(t)$ kinetics, two types of structures can be selected. When $I > 2\,\mathrm{mWcm}^{-2}$ the samples contain small LC domains (the average domain diameter $d$ is 0.5–5 μm) with high monodispersity. This is in good agreement with earlier studies of other groups [9,11] and our results obtained by SEM method [18]. In turn, when $I < 2\,\mathrm{mWcm}^{-2}$, along with small droplets, much bigger droplets ($d = 20$–50 μm) appear.

Based on microphotographs presented in Figure 3 one can plot $d$ vs. $I$ curves (Fig. 4). The dual size of LC drops at $I < 2\,\mathrm{mWcm}^{-2}$ results in splitting of $d(I)$ curve. Before the splitting, in the intensity range 4–40 mWcm$^{-2}$, the $d(I)$ curve exhibits rather slow decrease, which, similiar to [9,11], can be considered as a quasilinear one. The difference in PDLC morphologies formed at low ($I < 2\,\mathrm{mWcm}^{-2}$) and high ($I > 2\,\mathrm{mWcm}^{-2}$) intensity of curing light might be explained by different LC-polymer demixing mechanisms. At high intensities a gel point is rapidly reached so that LC and polymer separate mainly via the liquid-gel demixing with a high rate of prepolymer conversion [14]. This leads to formation of fine monodispersed drops. In
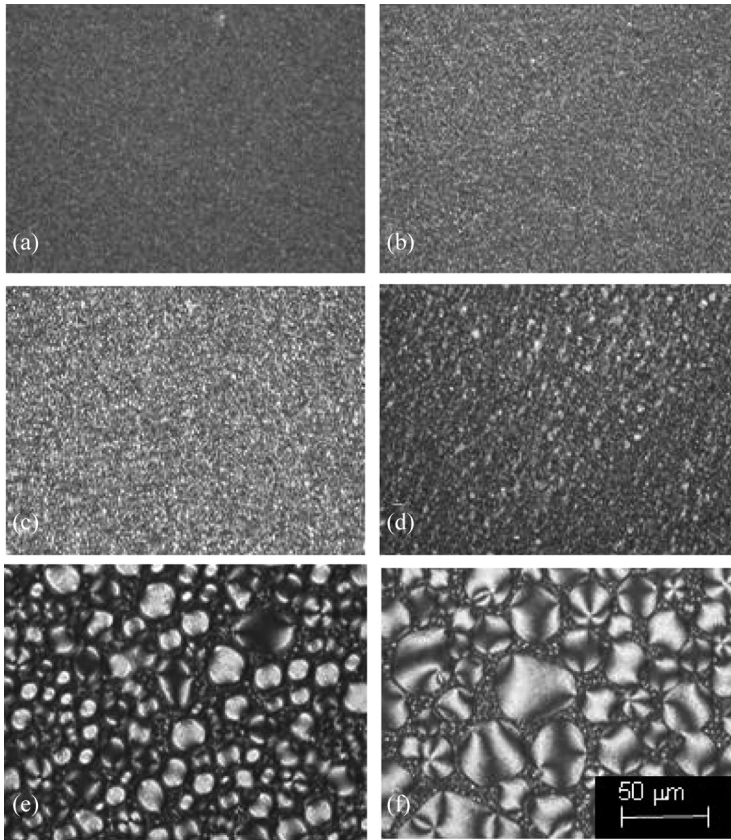
**Figure 3.** Microphotographs of PDLC samples obtained for different UV light intensities. The intensity is equal to 36, 18, 4, 2, 1.2 and $0.8\,\mathrm{mWcm^{-2}}$ in case (a), (b), (c), (d), (e) and (f), respectively. The exposure time is 70 s.
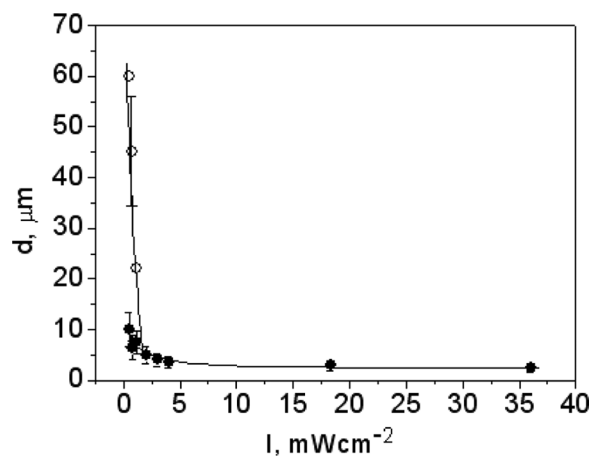


**Figure 4.** Diameter of segregated LC domains as a function of exposure light intensity. In case of dual-size morphologies realized at $I < 2\,\mathrm{mWcm^{-2}}$, the filled and open circles stand for droplets of smaller and bigger size, respectively. The exposure time is fixed at 70 s.

contrast, at low intensity of curing light the conversion process is slow. This means that the system arrives at a gel point slowly and thus, on the initial stage, the phase separation occurs mainly via the liquid-liquid demixing. The slow separation dynamics results in formation of relatively big LC domains capable to coalesce in a course and just after the illumination [21].

## 4. Conclusions

In this work, the photoinduced phase separation in the E7-NOA65 composites was studied in a wide intensity range of actinic UV light ($I = 0.5$–$40\,\mathrm{mWcm^{-2}}$). The phase separation process was monitored by measuring transmittance kinetics of the E7-NOA65 composite layers. In general, this process is rather complex; the transmittance vs. exposure time curves are satisfactorily fitted only by a stretched exponent (1) with a stretching parameter $\beta > 1$ approaching 1 at high UV light intensities. Increase of curing light intensity accelerates the phase separation and drastically influences the final structure of PDLC samples. Reduction of light intensity below $2\,\mathrm{mWcm^{-2}}$ results in the transition from the ordinary morphology of fine droplets to the morphology of prevailing big droplets with a size comparable or bigger than the thickness of the composite layer. This morphological transition is explained by a change in the prevailing mechanism of phase separation from the "liquid-gel" to the "liquid-liquid" one. The realized transition extends the field of PDLC morphologies of E7-NOA65 composites and thus the field of their potential applications. Particularly, effective controlling of droplet parameters by light intensity makes possible patterning of PDLC morphology and creation of morphologies with controllable gradient of droplet size. In addition to conventional (uniform) PDLC and holographic PDLC these modifications give additional options for information displaying and storage systems based on PDLC composites.

## Acknowledgments

## References

[1] Doane, J. W. (1990). Polymer dispersed liquid crystal displays. In: *Liquid Crystals Applications and Uses* 1, Bahadur, B. (Ed.), (Chapter 14), World Scientific: Singapore, 362–395.

[2] Drzaic, P. S. (1995). *Liquid Crystal Dispersions*. World Scientific: Singapore.

[3] Bouteiller, L., & Le Barny, P. (1996). *Liquid Crystals*, *21*(2), 157.

[4] Odian, G. (1991). *Principles of Polymerization*, 3rd ed., Wiley: New York.

[5] Natarajan, L. V., *et al.* (2003). *Chem. Mater.*, *15*, 2477.

[6] Nwabunma, D., *et al.* (1998). *Macromolecules*, *31*, 6806.

[7] Li, J., Baird, G., *et al.* (2005). *Journal of the SID*, *13*(12), 1019.

[8] Vaz, N. A., Smith, G. W., & Montgomery, G. P. (1987). *Mol. Cryst. Liq. Cryst.*, *146*, 1.

[9] Lackner, A. M., *et al.* (1989). *SPIE*, *1080*, 53.

[10] Smith, G. W. (1991). *Mol. Cryst. Liq. Cryst.*, *196*, 89.

[11] Erman, J. H., *et al.* (1993). *Journal of the SID*, *1*(1), 57.

[12] Bhargava, R., Wang, S-Q., & Koenig, J. (1999). *Macromolecules*, *32*, 2748.

[13] Bhargava, R., Wang, S-Q., & Koenig, J. (1999). *Macromolecules*, *32*, 8982.

[14] Bhargava, R., Wang, S-Q., & Koenig, J. (1999). *Macromolecules*, *32*, 8989.

[15] White, T. J., *et al*. (2007). *Macromolecules*, *40*(4), 1112.

[16] Yaroshchuk, O. V., Dolgov, L. O., & Kiselev, A. D. (2005). *Phys. Rev. E*, *72*, 051715.

[17] Yaroshchuk, O. V., & Dolgov, L. O. (2007). *Optical Materials*, *29*, 1097.

[18] Dolgov, L., Yaroshchuk, O., & Qiu, L. (2007). *Mol. Cryst. Liq. Cryst.*, *468*, 335.

[19] Méchernène, L., *et al*. (2009). *Opt. Materials*, *31*, 632.

[20] Alvarez, F., Alegría, A., & Colmenero, J. (1991). *Phys. Rev. B*, *44*, 7306.

[21] Carter, S. A., *et al*. (1997). *J. Appl. Phys.*, *81*(9), 5992.